Circularly polarized luminescence on dinuclear Tb(III) and Eu(III) complexes with (S-) and (R-) 2-phenylpropionate†

Berta Casanovas,[a] Francesco Zinna,[b] Lorenzo Di Bari, *[b] Mohamed Salah El Fallah,[a] Mercè Font-Bardía[c] and Ramon Vicente *[a]

aDepartament de Química Inorgànica i Orgànica, Secció de Química Inorgànica, Universitat de Barcelona, Martí i Franquès 1-11, 08028 Barcelona, Spain.
E-mail: rvicente@ub.edu
bDipartimento di Chimica e Chimica Industriale, Università di Pisa, via Moruzzi 13, I-56124 Pisa, Italy.
E-mail: lorenzo.dibari@unipi.it
cDepartament de Mineralogia, Cristallografia i Dipòsits Minerals and Unitat de Difracció de R-X, Centre Científic i Tecnològic de la Universitat de Barcelona (CCiTUB), Universitat de Barcelona, Solé i Sabarís 1-3, 08028 Barcelona, Spain

.

ABSTRACT:

The reaction of Ln(NO3)2·6H2O (Ln = Tb and Eu) with (S)-(+)-2-phenylpropionic acid (S-HL) and 1,10-phenanthroline (phen) in EtOH/H2O allows the isolation of the dinuclear chiral compounds of the formula [Ln2(S-L)6(phen)2]·2.5·S-HL in which Ln = Tb (S-1), Ln = Eu (S-2). The same synthesis by using (R)-(−)-2-phenylpropionic acid (R-HL) instead of (S)-(+)-2-phenylpropionic acid allows the isolation of the enantiomeric compounds with the formula [Ln2(R-L)6(phen)2]·2.5·R-HL where Ln = Tb (R-1), Ln = Eu (R-2). All compounds show sensitized luminescence. The luminescence study, including the circularly polarized luminescence spectra of the four compounds, is reported. The magnetic behavior of S-1 and S-2 is also reported.

INTRODUCTION

Currently, lanthanide compounds are mainly studied for their magnetic and luminescence properties. From the magnetic point of view, since the discovery of mononuclear lanthanide complexes functioning as single molecule magnets (SMMs),1 an increasing number of mono and polynuclear SMM complexes derived from lanthanide ions with large orbital momentum and strong magnetic anisotropy have been reported.2 On the other hand, luminescent lanthanide complexes are of interest due to their wide range of applications in materials and biosciences.3 Due to their potential use in nonlinear optics or circularly polarized luminescent materials, the preparation of chiral lanthanide coordination compounds is of high current interest.4

Moreover, the first observation of magnetochiral dichroism was made on the emission properties of a Eu complex5 and also recently there is significant interest in lanthanide compounds for studying magnetochiral effects.6 For similar applications, the simultaneous evaluation of magnetic and chiroptical properties of one complex is a necessary pre-requisite.

The reported examples of chiral lanthanide complexes are mainly limited to the mono- and bi-nuclear structures,7 although higher nuclearity systems were also reported.8 In general, three approaches are available for the introduction of chirality into metal complex assemblies: (i) spontaneous chiral symmetry breaking, (ii) chiral induction, and (iii) ligand chirality. We have used the ligand chirality approach to synthesize dinuclear 4f-metal ion complexes by employing simultaneously bidentate bridging carboxylate ligands generated from (S)-(+)- or (R)-(−)-2-phenylpropionic acid (S- and R-HL respectively) with neutral chelating 1,10-phenanthroline ligands which block two coordination sites per Ln(III) ion and terminate further aggregation or potential polymerization. The 1,10-phenanthroline ligands also play the role of sensitizing the luminescence of the lanthanide ion, through the so-called antenna effect. In fact, because of the weak f–f absorption of trivalent lanthanide ions, a suitable chromophoric organic ligand should be employed to populate the lanthanide emitting states through an energy transfer process.9

The chiral ligands naturally induce a dissymmetric environment around Ln(III), which determines the onset of chiroptical properties allied to the f–f transitions of the ion. In emission this is sensitively monitored through circularly polarized luminescence (CPL), which can be conveniently quantified by means of the dissymmetry factor glum:

$$g_{\mathrm{lum}} = 2\frac{I_{\mathrm{L}} - I_{\mathrm{R}}}{I_{\mathrm{L}} + I_{\mathrm{R}}} = \frac{\Delta I}{I}$$

where IL and IR are the left and right circularly polarized components of the emission.

Usually non-aggregated organic molecules or d-metal complexes display glum factors of the order of 10−4–10−3,10 while much higher values (10−1–1)11 are reported for lanthanide complexes. For such outstanding CPL properties, chiral Ln complexes are used in several applications such as responsive bioprobes12 or more recently in electronic devices able to directly emit circularly polarized electroluminescence.13 Usually, CPL is measured for mononuclear Eu complexes, while reports of CPL from complexes with higher nuclearity, such as binuclear helicates14 or trinuclear15 and heptanuclear16 systems, remain rare.

Moreover, polydentate and often macrocyclic ligands are commonly used in this context,17 while to the best of our knowledge, simple monofunctional (i.e. monotopic) chiral carboxylates seem to be unprecedented in this context.

.

EXPERIMENTAL SECTION

Starting materials

Ln(NO3)3·6H2O salts, (S)-(+)- or (R)-(−)-2-phenylpropionic acid and 1,10-phenanthroline (Aldrich) were used as received.

Synthesis

Preparation of dinuclear complexes [Ln2(R/S-L)6(phen)2]2· 2.5·R/SHL (S/R-1–S/R-2). The preparation of compounds S/R-1–S/R-2 was achieved via the reactions of the corresponding enantiomerically pure (S)-(+)- or (R)-(−)-2-phenylpropionic acid (S or R-HL, 1.5 mmol) and 1,10-phenanthroline (phen, 0.3 mmol) dissolved in 20 mL of EtOH/H2O (v/v = 50 : 50) with a solution of 0.25 mmol of the corresponding Ln(NO3)3·6H2O salt in 10 mL of EtOH (S-HL and Ln = Tb in S-1, S-HL and Ln = Eu in S-2, R-HL and Ln = Tb in R-1, R-HL and Ln = Eu in R-2). The mixture was stirred for 1 hour at room temperature. Good crystals suitable for X-ray analysis of compounds S/R-1–S/R-2 were obtained within 5–10 days after the slow evaporation of the mixture. Anal. calc. (%) for S-1 C, 61.94; H, 4.91; N, 2.87. Found: C, 62.7; H, 5.4; N, 2.9, calc. (%) for S-2 C, 62.39; H, 4.95; N, 3.19. Found: C, 62.4; H, 5.1; N, 3.2, calc. (%) for R-1 C, 61.94; H, 4.91; N, 2.87. Found: C, 62.4; H, 5.3; N, 3.0. calc. (%) for R-2 C, 62.39; H, 4.95; N, 3.19. Found: C, 63.5; H, 5.4; N, 2.9.

IR and magnetic measurements

Infrared spectra (4000–400 cm−1) were recorded from KBr pellets on a PerkinElmer 380-B spectrophotometer.

Magnetic measurements were performed on solid polycrystalline samples with a Quantum Design MPMS-XL SQUID magnetometer at the Magnetic Measurements Unit of the University of Barcelona. Pascal's constants were used to estimate the diamagnetic corrections, which were subtracted from the experimental susceptibilities to give the corrected molar magnetic susceptibilities.

Chiroptical spectroscopy measurements

ECD spectra. ECD spectra were recorded with a Jasco J-710 spectropolarimeter on the same samples used for CPL measurements. In order to rule out the occurrence of contributions from linear dichroism/linear birefringence, different spectra recorded after rotating the sample by 90° around the optical axis or around an axis perpendicular to the optical axis were recorded and compared; all the spectra were averaged.

CPL spectra. We ran simultaneously the fluorescence and circularly polarized luminescence measurements with our home-built CPL spectrofluoropolarimeter18 under UV irradiation (λmax = 365 nm) on quartz plate depositions. The depositions of the complexes were obtained from CH3CN dispersions. CH3CN was chosen as a dispersant because it does not dissolve compounds S/R-1–S/R-2,

in this way the complexes are deposited as a microcrystalline powder film (see Fig. S4a and S4b†). This ensures that the complexes do not change their structures, as it happens in solution (see Results and discussion). Several spectra were acquired rotating the sample as described above for ECD.

X-ray crystallography

Good quality crystals of S/R-1–S/R-2 were selected and mounted on a D8VENTURE (Bruker) diffractometer with a CMOS detector. The crystallographic data, conditions retained for the intensity data collection, and some features of the structure refinements are listed in Table 1. All the structures were refined by the least-squares method. Intensities were collected with multilayer monochromated Mo-Kα radiation. Lorentz polarization and absorption corrections were made for S/R-1–S/R-2. The structures were solved by direct methods, using the SHELXS-97 computer program19 and refined by the full-matrix least-squares method, using the SHELXL-2014 computer program.20 The non-hydrogen atoms were located in successive difference Fourier syntheses and refined with anisotropic thermal parameters on F2. For hydrogen atoms isotropic temperature factors have been assigned as 1.2 or 1.5 times the respective parent.

NMR spectra

NMR spectroscopy was performed with an Agilent INOVA 600 spectrometer operating at 600 MHz for 1H. Temperature was set to 25.0 ± 0.1 °C. The spectra were measured in CDCl3.

RESULTS AND DISCUSSION

General syntheses

The solvothermal method has been extensively employed to produce polymeric lanthanide compounds with bridging carboxylate ligands with diverse interesting structures although the mechanism is not completely clear so far.3a In our experiment, we used a straightforward room temperature synthetic procedure avoiding the solvothermal process.

Complexes S/R-1–S/R-2 exhibit very similar IR spectra and, thus, only the IR spectrum of S-1 will be discussed. The characteristic bands of carboxyl groups appear at 1599 cm−1 for asymmetric stretching (vas) and 1426 cm−1 for symmetric stretching (vs). Absorption bands observed in the range 3060–2934 cm−1 are ascribed to the C–H stretching from the methyl group of S-(+)-2-phenylpropionate. In addition, the presence of a strong absorption peak at 1725 cm−1 (–COOH) and a broad band at 3433 cm−1 (ν(O–H)) confirms the presence of the protonated S-HL ligand.

Molecular structures of S/R-1–S/R-2

Single-crystal X-ray analysis of complexes S/R-1–S/R-2 reveals that all the complexes crystallize in the monoclinic P21 space group. The asymmetric unit of S/R-1–S/R-2 consists of two dinuclear [Ln2(R/S-L)6(phen)2] units named A and B. The difference between the dinuclear A–B entities increases based on the number and the acceptor oxygen atom of the hydrogen bonds with the five S-HL or R-HL non-coordinated ligands. Molecule A exhibits two hydrogen bonds at O9A and O11A, meanwhile molecule B forms three hydrogen bonds with O9B, O11B and O12B for compounds S-1 and S-2 (S-L), and with O10B, O11B and O12B for compounds R-1 and R-2 (R-L). The hydrogen bonds between the dinuclear entities and the S- or R-HL carboxylic acids do not promote 1D, 2D or 3D supramolecular arrangement between the dinuclear fragments.

As mentioned above, S/R-1–S/R-2 exhibit the same structure with only differences in the structural parameters and thus, only the structure of dinuclear unit A from compound S-1 will be discussed. [Tb2(S-L)6(phen)2]·2.5·S-HL (S-1) A labelled plot of the structure of the dinuclear fragment A of compound S-1 is shown in Fig. 1. Selected bond distances of the dinuclear fragment A for S/R-1–S/R-2 are listed in Table 2. The same structural parameters for the fragment B and hydrogen bonds and angles for all compounds are given in Tables S1 and S2† respectively.

The structure consists of dinuclear molecules in which each Tb(III) is TbN2O7 nonacoordinated (Fig. 2).

In each unit, the two Tb(III) atoms are bridged through four (S)-(+)-2-phenylpropionate ligands, Fig. 1 and Scheme 1. The Tb1A···Tb2A distance is 3.963 Å. There are two different kinds of coordination modes for the bridging ligands (Scheme 2). One of them is a symmetrical syn,syn bridge (η1:η1:μ or 2.11 using Harris notation) (Scheme 2a) with the Tb1A–O1A, Tb1A–O5A, Tb2A–O2A, Tb2A–O6A bond lengths being 2.317(4), 2.339(4), 2.363(4) and 2.330(4) Å, respectively. The second kind of (S)-

(+)-2-phenylpropionate bridging ligand is best described as chelating–bridging (η1:η2:μ or 2.21), Scheme 2b, in which O3A and O7A act as bridges between the two Tb atoms with distances of 2.869(4) for Tb1A–O3A, 2.343(4) Å for Tb2A–O3A, 2.610(4) for Tb2A–O7A and 2.324(4) Å for Tb1A–O7A, meanwhile O4A and O8A are bonded only with a Tb atom with distances for Tb1A–O4A and Tb2A–O8A of 2.365(4) and 2.433(4) Å respectively. The coordination sphere of each metal is completed by the two N atoms of the 1,10-phenanthroline ligand with bond lengths of Tb1A–N1A, Tb1A–N2A, Tb2A–N3A and Tb2A–N4A of 2.545(5), 2.579(5), 2.608(5) and 2.576(5) Å, respectively, and by the two carboxylic oxygen atoms from terminal chelating (S)-(+)-2-phenylpropionate anions, Scheme 2c, with bond lengths for Tb1A–O9A, Tb1A–O10A, Tb2A–O11A and Tb2A–O12A of 2.479(4), 2.446(4), 2.465(4) and 2.439(4) Å respectively. The hydrogen bonds between the complex and the ligand do not promote 2D or 3D supramolecular arrangement.

Magnetic properties

Solid-state direct-current (dc) magnetic susceptibility (χM) data on the powder samples of complexes S-1 and S-2 were collected under the applied fields of 0.3 T (300–2.0 K) and 0.5 T (300–2.0 K), respectively. The data are plotted as χMT products versus T in Fig. 3. Magnetization dependence of the applied field at 2 K for compounds S-1 and S-2 is shown in Fig. 4a and b, respectively.

The room-temperature value of χMT for S-1 is 23.62 cm3 K mol−1, in good agreement for the calculated values of two free Tb(III) ions with the 7F6 ground state (23.64 cm3 K mol−1).3a The value of the χMT product remains almost constant down to ∼50 K and then decreases to 13.02 cm3 K mol−1 at 2.0 K. This behaviour can be attributed to weak antiferromagnetic interactions between the metal centers of the same dinuclear unit (the hydrogen bonds offered by the S- or R-HL molecules do not connect the dinuclear entities) in conjunction with a thermal depopulation of the mJ sublevels of the Tb(III) ion, which arise from the splitting of the ground term by the ligand field in Ln(III) ions with an unquenched orbital momentum. 21 The magnetization in front of the applied field in compound S-1 reaches a maximum value of 10.12NμB at 5 T. The non-saturation of the magnetization is due to the magnetic anisotropy of the Tb(III) ion and/or to the partially populated excited states.22

Compound S-2 presents a χMT of 2.67 at 300 K, a lower value than expected for two Eu(III) free isolated ions (3.06 cm3 K mol−1).3a,23 With cooling, χMT decreases gradually, reaching a value of 0.04 cm3 K mol−1 at 2 K, which should be explained through the depopulation of the excited states (7FJ=1–6) to the ground state 7F0.23 Magnetization measurements for complex S-2 show a value of 0.1NμB under an applied field of 5 T without saturation.

With the aim to investigate whether Tb(III) complexes show slow relaxation of the magnetization, alternating-current (ac) magnetic measurements for compound S-1 were performed on polycrystalline samples in the 2–10 K range and under a dc field of 0, 1500, 2000, 3000 and 4000 G with an ac field oscillating at 10 and 1000 Hz (Fig. S1†). No maxima in the out-ofphase (χ″M) signal were observed without the static applied field, as a consequence of the low energy barrier of the flipping of the

magnetization, not energetically high enough to maintain single configuration of the magnetization24 or due to the quantum tunnelling of magnetization effect (QTM) on the diminution of the energy barrier.25 Frequency dependence of the susceptibility for compound S-1 is observed under high dc applied fields (>2000 G) but without a net maximum above 2 K demonstrating that the QTM effect is not completely vanished.

Photophysical studies: emission spectral analysis

Circular dichroism. Electronic circular dichroism (ECD) spectra in the solid state of complexes S-1 and R-1 and S-2–R-2 are shown in Fig. 5 and 6, respectively, and display rather weak Cotton effects. In the ECD spectra of Tb(III) compounds S-1 and R-1, the bands between 320 and 360 nm can be assigned to Tb f → f transitions (probably 7F4 → 5D3/5G5/5D2). Only a small contribution from the 1,10-phenanthroline ligands is visible, despite 1,10-phenanthroline transitions having a much greater absorption cross section than Ln(III) ones. Similarly, in the ECD spectra of Eu(III) compounds S-2, R-2, the bands around 300 nm can be attributed to f → f transitions, since their width and spacing are not compatible with 1,10-phenanthroline transitions.

Emission spectra analysis. Emission spectra of microcrystalline compounds S/R-1–S/R-2 on a quartz plate deposition (λex = 365 nm) at room temperature are shown in Fig. 7 and 8. The corresponding solid state absorption spectra are shown in Fig. S2 and S3,† respectively. The sensitized Ln(III) based luminescence from the 1,10-phenanthroline ligand leads to the observation of the f–f transition of Tb(III) complexes S-1 and R-1 (Fig. 7). The spectra show the corresponding emission peaks due to the electronic transitions from the excited spectroscopic level 5D4 to the fundamental sublevels 7FJ at 489 (J = 6), 544 (J = 5), 584 (J = 4) and 620 nm (J = 3). The emission peaks from the 1,10-phenanthroline antenna ligand are not observed confirming the efficiency of the phen-Ln energy transfer process (Fig. S4c†). Similarly, upon exciting 1,10-phenanthroline at 365 nm, the Eu(III) compounds S-2 and R-2 (Fig. 8) display a set of transitions 5D0 → 7FJ at λem = 579 nm (J = 0), 592 nm (J = 1), 614 nm (hypersensitive transition J = 2), 656 nm (J = 3) and 697 (J = 4). The 5D0 → 7F2 hypersensitive transition is electric-dipole allowed and can be extremely sensitive to the geometry of the first coordination sphere of the Eu center.26 On the contrary the magnetic dipole transition 5D0 → 7F1 at 592 nm is rather insensitive to the coordination environment and provides a normalization to the hypersensitive transition. The fact that the total emission is stronger at 614 nm than at 593 nm indicates that the coordination sphere of Eu(III) does not present an inversion center.27 The emission shows only one peak for the 5D0 → 7F0 transition indicating the presence of a single chemical environment around the Eu(III) ion. As in the Tb(III) compound, the sensitization from the ligand to Eu(III) is nearly complete as also in this case no ligand based emission bands are observed. Is it worth noting that the emission spectra recorded on quartz plate depositions, casted from acetonitrile dispersion (Fig. 7 and 8), closely retrace the spectra measured on the crystalline powder (Fig. S4a and b†), thus confirming that the crystal structure and packing do not change significantly upon dispersing the sample in acetonitrile.

The solid state CPL spectra of Tb(III) compounds S-1 and R-1 appear rather weak but measurable, yielding the expected mirror image spectra for the two enantiomers (Fig. 9). Only the CPL of the most intense 5D4 → 7F5 band at 544 nm is reliably detectable. The glum factor of this band is around ±3.5 × 10−3 (see Table 3).

The CPL spectra of Eu(III) compounds S-2 and R-2 display mirror image bands corresponding to 5D0 → 7FJ (J = 1,2,4) transitions (Fig. 10).

The luminescence spectrum in Fig. 8 clearly shows that the hypersensitive transitions have at least two resolved components. In the CPL spectrum (Fig. 10) all the 2J + 1 components of the 5D0 → 7F2 manifold can be recognized. Indeed, the couplet-like structure around 617 nm displays two bands in the lower energy region (negative component compound S-2) and a bifid structure in the higher energy region (exactly reproduced in the mirror image by the enantiomer R-2). This structure calls for at least three unresolved bands with different signs (negative–positive–negative for the S enantiomer, compound S-2). This is again consistent with a low symmetry coordination environment.

Interestingly, the 5D0 → 7F1 transition is less intense than the hypersensitive transition in terms of glum, (Table 3). Usually the magnetically allowed-electrically forbidden 5D0 → 7F1 transition yields a higher glum than forced electrical dipole transitions (including 5D0 → 7F2). An explanation for this unusual behaviour may lie in the fact that up to 3 non-degenerate transitions can be hidden under the band around 593 nm in a C2 environment. It is possible that these unresolved transitions have opposite signs, partially cancelling out the total intensity of this band.

At this point, we investigated the CPL properties of the same compounds in CH2Cl2 solution. Interestingly, under such conditions the CPL spectra of both Tb(III) and Eu(III) are significantly different from the ones measured on the deposition.

In the case of Tb compounds a bright green luminescence and a rather strong CPL spectrum (Fig. S5†) can be recorded. The dominant feature is again the band around 544 nm. This transition displays a rich CPL spectrum with a glum factor of about ±1.6 × 10−2, higher than the solid state value by almost an order of magnitude.

Again, in the case of Eu(III) compounds (Fig. S6†), the CPL spectra show a relatively intense couplet-like band around 593 nm (5D0 → 7F1) with a glum factor about ±2.5 × 10−2. The glum corresponding to the 5D0 → 7F2 transition is of the order of magnitude of 10−3.

The differences between the CPL spectra in solution and in the solid state are a strong indication that the geometry of the complexes in the solid state determined by X-ray diffraction undergoes a deep change upon dissolution in a good solvent. It is known that Ln complexes can undergo a wealth of fast equilibria in solution, losing the well-ordered crystal structure.

In order to obtain a deeper insight into the processes that such compounds undergo in solution, we recorded the 1H-NMR spectra of Eu2 and Tb2 complexes in CDCl3. In both cases, the NMR spectra display very broad bands (HWHM ≈ 1000–10 000 Hz). This confirms the fluxional nature of the compounds and the presence of more than one species in fast/intermediate equilibrium on the NMR time

scale in solution (Fig. S7 and S8†). In all the spectra, the resonances due to the unbound (S)-(+)- or (R)-(−)-2-phenylpropionic acid ligand are clearly visible, while the unbound 1,10-phenanthroline bands are not visible in the case of Tb. In the Eu spectrum instead, they are visible but their relative intensity is much smaller than expected from the intensity of free (S)-(+)- or (R)-(−)-2- phenylpropionic acid signals.

This suggests that in all cases, most of the 1,10-phenanthroline is complexed with the lanthanide. This is in agreement with CPL data. Indeed, since it is possible to measure luminescence and CPL spectra also in solution under 365 nm irradiation, it is necessary that each Ln(III) giving rise to a CPL signal interacts with both 1,10-phenanthroline (acting as the sensitizer) and (S)-(+)- or (R)-(−)-2-phenylpropionic acid (acting as the chirality source).

CONCLUSIONS

We have successfully isolated dinuclear chiral compounds of the formula [Ln2(S-L)6(phen)2]·2.5S-HL in which Ln = Tb (S-1), Ln = Eu (S-2) and [Ln2(R-L)6(phen)2]·2.5R-HL where Ln = Tb (R-1), Ln = Eu (R-2). S/R-HL = (S)-(+)- and (R)-(−)-phenylpropionic acid respectively. Magnetic and luminescence studies of compounds S-2 and S-2 indicate the ground states 7F6 for Tb(III) and 7F0 for Eu(III) centres. In the Tb(III) compounds ac magnetic measurements have been carried out showing the frequency dependence of $\chi''M$ only under very high dc fields demonstrating that the QTM is not completely vanished. The neutral chelating 1,10-phenanthroline ligands block two coordination sites per Ln(III) ion and terminate further aggregation or potential polymerization, playing also the role of sensitizing the luminescence of the lanthanide ion, through the so-called antenna effect. S/R-1–S/R-2 show sensitized luminescence. We have reported the luminescence study of the new chiral compounds including the circularly polarized luminescence spectra of S/R-1–S/R-2. Usually, CPL is measured for mononuclear Eu complexes, while reports of CPL from complexes with higher nuclearity, such as binuclear helicates14 or trinuclear15 and heptanuclear16 systems, remain rare. Moreover, in the context of chiral luminescent complexes commonly polydentate and often macrocyclic ligands have been used,17 while to the best of our knowledge, simple monofunctional (i.e. monotopic) chiral carboxylates seem to be unprecedented.

ACKNOWLEDGEMENTS

R. V. acknowledges the financial support from the Spanish government grant CTQ2015-63614-P.

REFERENCES

1 N. Ishikawa, M. Sugita, T. Ishikawa, S. Y. Koshihara and Y. Kaizu, J. Am. Chem. Soc., 2003, 125, 8694.

2 (a) J. Tang and P. Zhang, Lanthanide Single Molecule Magnets, Springer-Verlag, Berlin, Heidelberg, 2015; (b) H. L. C. Feltham and S. Brooker, Coord. Chem. Rev., 2014, 276, 1; (c) D. N. Woodruff, R. E. P. Winpenny and R. A. Layfield, Chem. Rev., 2013, 113, 5110.

3 (a) The Rare Earth Elements, Fundamentals and Applications, ed. D. A. Atwood, John Wiley& Sons Ltd, 2012; (b) Z. Xia, Z. Xu, M. Chen and Q. Liu, Dalton Trans., 2016, 45, 11214; (c) J.-C. G. Bünzli and C. Piguet, Chem. Soc. Rev., 2005, 34, 1048; (d) J.-C. G. Bünzli, Acc. Chem. Res., 2006, 39, 53; (e) S. Swavey and R. Swavey, Coord. Chem. Rev., 2009, 253, 2627; (f) S. V. Eliseeva and J.-C. G. Bünzli, Chem. Soc. Rev., 2010, 39, 189; (g) E. G. Moore, A. P. S. Samuel and K. N. Raymond, Acc. Chem. Res., 2009, 42, 542; (h) C. P. Montgomery, B. S. Murray, E. J. New, R. Pal and D. Parker, Acc. Chem. Res., 2009, 42, 925; (i) S. J. Butler, M. Delbianco, L. Lamarque, B. K. McMahon, E. R. Neil, R. Pal, D. Parker, J. W. Walton and J. M. Zwier, DaltonTrans., 2015, 44, 4791.

4 (a) G. Koeckelberghs, S. Sioncke, T. Verbiest, A. Persoons and C. Samyn, Chem. Mater., 2003, 15, 2870; (b) S. Dang, J.-H. Zhang, Z.-M. Sun and H.-J. Zhang, Chem. Commun., 2012, 48, 11139; (c) E. Peeters, M. P. T. Christiaans, R. A. J. Janssen, H. F. M. Schoo, H. P. J. M. Dekkers and E. W. Meijer, J. Am. Chem. Soc., 1997, 119, 9909; (d) J. P. Leonard, P. Jensen, T. McCabe, J. E. O'Brien, R. D. Peacock, P. E. Kruger and T. Gunnlaugsson, J. Am. Chem. Soc., 2007, 129, 10986; (e) F. Stomeo, C. Lincheneau, J. P. Leonard, J. E. O'Brien, R. D. Peacock, C. P. McCoy and T. Gunnlaugsson, J. Am. Chem. Soc., 2009, 131, 9636.

5 G. L. J. A. Rikken and E. Raupach, Nature, 1997, 390, 493.

6 I. Mihalcea, M. Perfetti, F. Pineider, L. Tesi, V. Mereacre, F. Wilhelm, A. Rogalev, C. E. Anson, A. K. Powell and R. Sessoli, Inorg. Chem., 2016, 55, 10068.

7 (a) J. P. Leonard, P. Jensen, T. McCabe, J. E. O'Brien, R. D. Peacock, P. E. Kruger and T. Gunnlaugsson, J. Am. Chem. Soc., 2007, 129, 10986; (b) F. Stomeo, C. Lincheneau, J. P. Leonard, J. E. O'Brien, R. D. Peacock, C. P. McCoy and T. Gunnlaugsson, J. Am. Chem. Soc., 2009, 131, 9636; (c) C. Lincheneau, C. Destribats, D. E. Barry, J. A. Kitchen, R. D. Peacockb and T. Gunnlaugsson, Dalton Trans., 2011, 40, 12056; (d) C.-T. Yeung, W. T. K. Chan, S.-C. Yan, K.-L. Yu, K.-H. Yim, W.-T. Wong and G.-L. Law, Chem. Commun., 2015, 51, 592.

8 (a) M. Lama, O. Mamula, G. S. Kottas, L. De Cola, H. Stoeckli-Evans and S. Shova, Inorg. Chem., 2008, 47, 8000; (b) G. Bozoklu, C. Gateau, D. Imbert, J. Pécaut, K. Robeyns, Y. Filinchuk, F. Memon, G. Muller and M. Mazzanti, J. Am. Chem. Soc., 2012, 134, 8372.

9 (a) K. Miyata, Y. Konno, T. Nakanishi, A. Kobayashi, M. Kato, K. Fushimi and Y. Hasegawa, Angew. Chem., Int. Ed., 2013, 52, 6413; (b) Y. Kuramochi, T. Nakagawa, T. Yokoo, J. Yuasa,

T. Kawaia and Y. Hasegawa, Dalton Trans., 2012, 41, 6634; (c) H. Xin, F.-Y. Li, M. Shi, Z.-Q. Bian and C.-H. Huang, J. Am. Chem. Soc., 2003, 125, 7166; (d) A. P. Bassett, S. W. Magennis, P. B. Glover, D. J. Lewis, N. Spencer, S. Parsons, R. M. Williams, L. D. Cola and Z. Pikramenou, J. Am. Chem. Soc., 2004, 126, 9413; (e) X.-P. Yang, R. A. Jones and S.-M. Huang, Coord. Chem. Rev., 2014, 273, 63; (f) M. Tropiano, N. L. Kilah, M. Morten, H. Rahman, J. J. Davis, P. D. Beer and S. Faulkner, J. Am. Chem. Soc., 2011, 133, 11847; (g) J. D. Moore, R. L. Lord, G. A. Cisneros and M. J. Allen, J. Am. Chem. Soc., 2012, 134, 17372; (h) B. Alpha, J.-M. Lehn and G. Mathis, Angew. Chem., Int. Ed. Engl., 1987, 26, 266; (i) C. Bazzicalupi, A. Bencini, A. Bianchi, C. Giorgi, V. Fusi, A. Masotti, B. Valtancoli, A. Roque and F. Pina, Chem. Commun., 2000, 561.

10 E. M. Sánchez-Carnerero, A. R. Agarrabeitia, F. Moreno, B. L. Maroto, G. Muller, M. J. Ortiz and S. de la Moya, Chem. – Eur. J., 2015, 21, 13488.

11 (a) F. Zinna and L. Di Bari, Chirality, 2015, 27, 1; (b) J. L. Lunkley, D. Shirotani, K. Yamanari, S. Kaizaki and G. Muller, Inorg. Chem., 2011, 50, 12724; (c) F. Zinna, C. Resta, S. Abbate, E. Castiglioni, G. Longhi, P. Mineo and L. Di Bari, Chem. Commun., 2015, 51, 11903.

12 (a) C. P. Montgomery, B. S. Murray, E. J. New, R. Pal and D. Parker, Acc. Chem. Res., 2009, 42, 925; (b) R. Carr, N. H. Evans and D. Parker, Chem. Soc. Rev., 2012, 41, 7673.

13 (a) F. Zinna, U. Giovanella and L. Di Bari, Adv. Mater., 2015, 27, 1791; (b) F. Zinna, M. Pasini, F. Galeotti, C. Botta, L. Di Bari and U. Giovanella, Adv. Funct. Mater., 2017, 27, 1603719.

14 (a) M. Cantuel, G. Bernardinelli, G. Muller, J. P. Riehl and C. Piguet, Inorg. Chem., 2004, 43, 1840; (b) F. Stomeo, C. Lincheneau, J. P. Leonard, J. E. OBrien, R. D. Peacock, C. P. McCoy and T. Gunnlaugsson, J. Am. Chem. Soc., 2009, 31, 9636.

15 (a) O. Mamula, M. Lama, S. G. Telfer, A. Nakamura, R. Kuroda, H. Stoeckli-Evans and R. Scopelitti, Angew. Chem., Int. Ed., 2005, 117, 2583; (b) M. Lama, O. Mamula, G. S. Kottas, F. Rizzo, L. De Cola, A. Nakamura, R. Kuroda and H. Stoeckli-Evans, Chem. – Eur. J., 2007, 13, 7358.

16 G. Bozoklu, C. Gateau, D. Imbert, J. Pecaut, K. Robeyns, Y. Filinchuk, F. Memon, G. Muller and M. Mazzanti, J. Am. Chem. Soc., 2012, 134, 8372.

17 G. Muller, Dalton Trans., 2009, 9692.

18 F. Zinna, T. Bruhn, C. A. Guido, J. Ahrens, M. Broring, L. Di Bari and G. Pescitelli, Chem. – Eur. J., 2016, 22, 16089.

19 G. M. Sheldrick, Acta Crystallogr., Sect. A: Fundam. Crystallogr., 2008, 64, 112.

20 G. M. Sheldrick, Acta Crystallogr., Sect. C: Cryst. Struct. Commun., 2015, 71, 3.

21 E. Colacio, J. Ruiz, A. J. Mota, M. A. Palacios, E. Cremades, E. Ruiz, F. J. White and E. K. Brechin, Inorg. Chem., 2012, 51, 5857.

22 P. Bag, C. K. Rastogi, S. Biswas, S. Sivakumar, V. Mereacre and V. Chandrasekhar, Dalton Trans., 2015, 44, 4328.

403 23 X. Mei, X. Wang, J. Wang, Y. Ma, L. Li and D. Liao, NewJ. Chem., 2013, 37, 3620.
404 24 M. A. Palacios, S. Titos-Padilla, J. Ruiz, J. M. Herrera, S. J. A. Pope, E. K. Brechin and E.
405 Colacio, Inorg. Chem., 2014, 53, 1465.
406 25 S. Biswas, S. Das, G. Rogez and V. Chandrasekhar, Eur. J. Inorg. Chem., 2016, 3322.
407 26 D. B. Ambili Raj, B. Francis, M. L. P. Reddy, R. R. Butorac, V. M. Lynch and A. H. Cowley,
408 Inorg. Chem., 2010, 49, 9055.
409 27 A. R. Ramya, M. L. P. Reddy, A. H. Cowley and K. V. Vasudevan, Inorg. Chem., 2010, 49,
410 2407.
411

Legends to figures

Figure. 1 Partially labeled plot of fragment A from compound S-1.

Figure. 2 Coordination polyhedron of the Tb(III) ions in S-1A.

Scheme 1 Partially labeled diagram of the dinuclear fragment of compound S-1.

Scheme 2 Coordination modes of the S/R-2-phenylpropionate ligand.

Figure. 3 χMT vs. T plot for compounds S-1 and S-2.

Figure. 4 Magnetization vs. applied field in Gauss at 2 K for compounds S-1 (a) and S-2 (b).

Figure 5. Solid state ECD spectra of S-1 and R-1 complexes.

Figure 6 Solid state ECD spectra of S-2 and R-2 complexes.

Figure 7 Solid state emission spectra of Tb(III) complexes S-1 and R-1 on a quartz plate deposition.

Figure 8 Solid state emission spectra of Eu(III) complexes S-2 and R-2 on a quartz plate deposition.

Figure 9 Solid state CPL spectra of Tb(III) complexes S-1 and R-1 on a quartz plate deposition.

Figure 10 Solid state CPL spectra of Eu(III) complexes S-2 and R-2 on a quartz plate deposition.

FIGURE 1

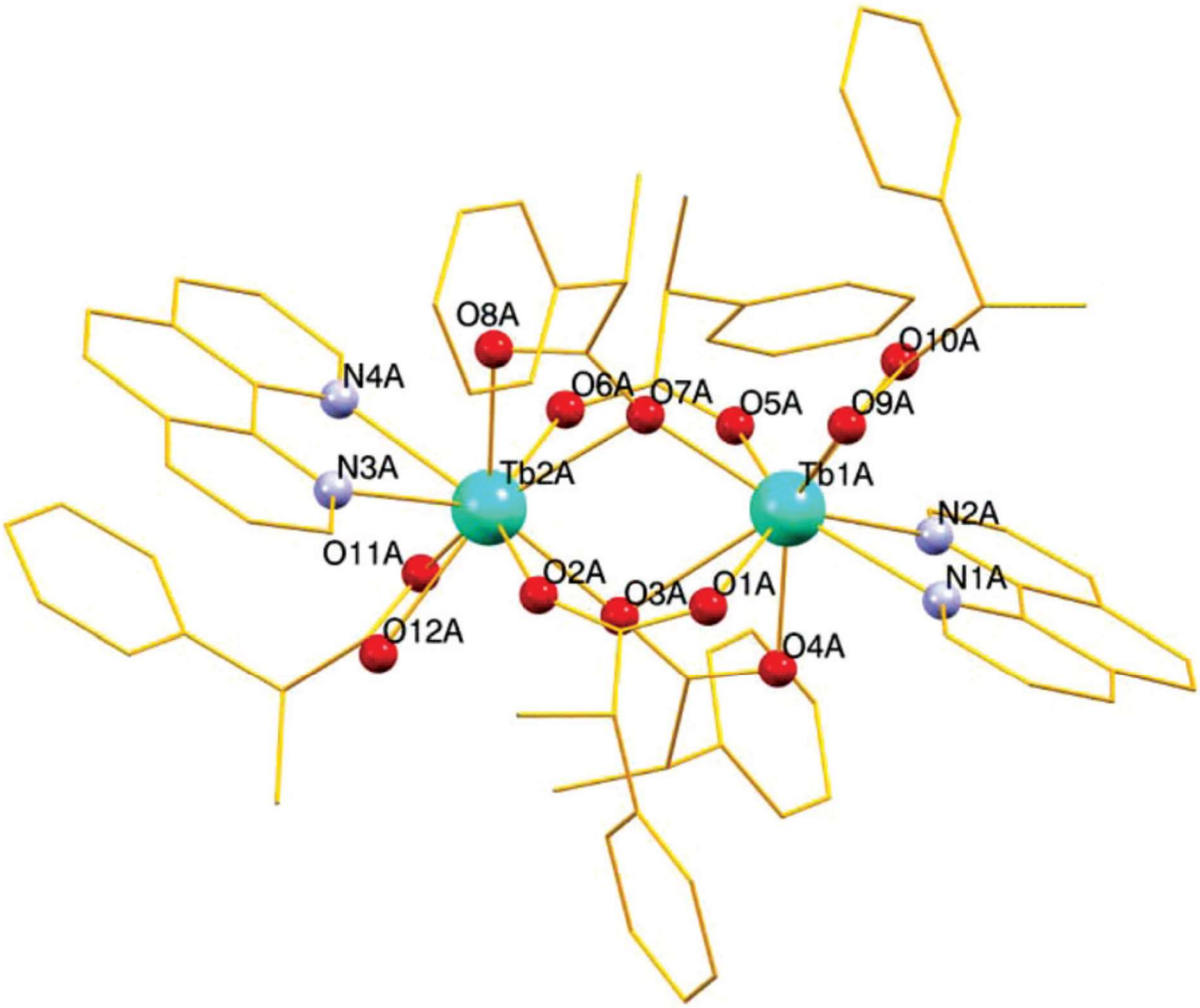
O8A
N4A
O6A
O7A
O5A
O10A
O9A
N3A
Tb2A
Tb1A
N2A
O11A
O2A
O3A
O1A
N1A
O12A
O4A

444 **FIGURE 2**

445

446

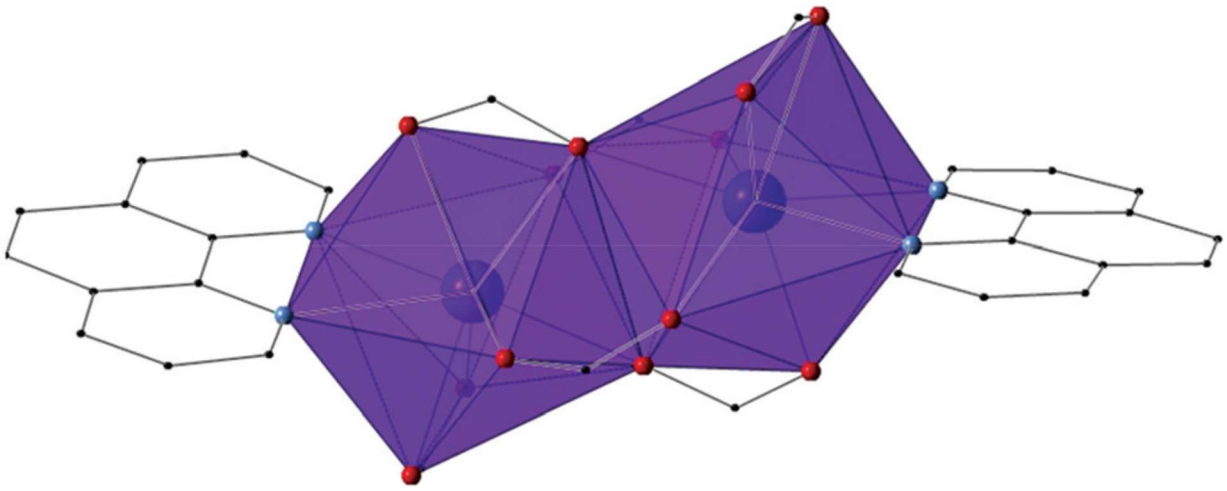

447

448

SCHEM 1

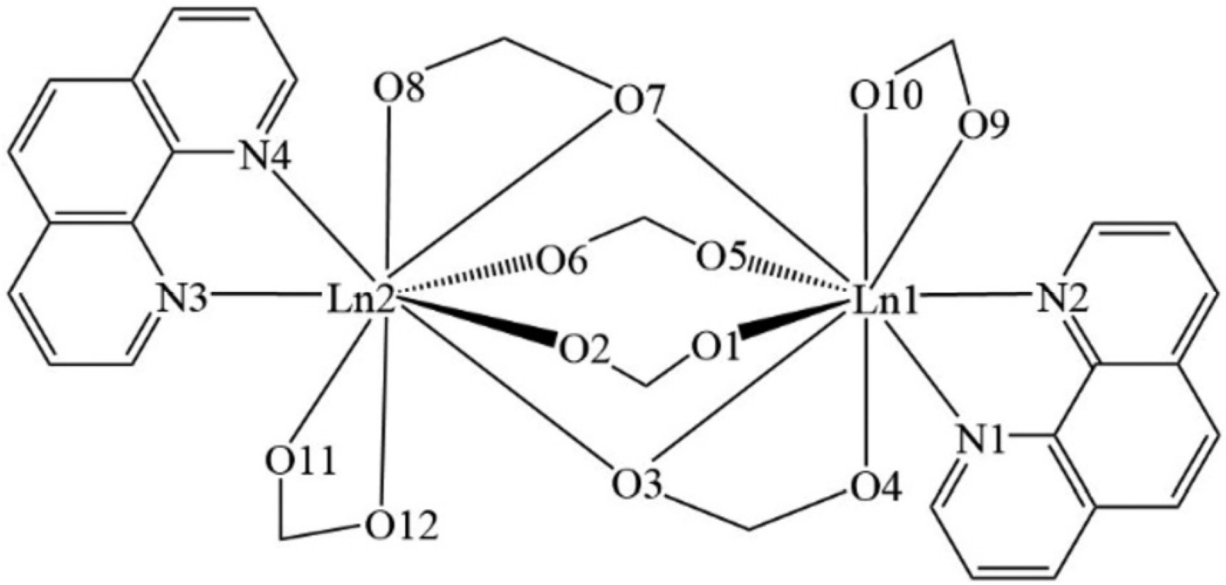

SCHEM 2

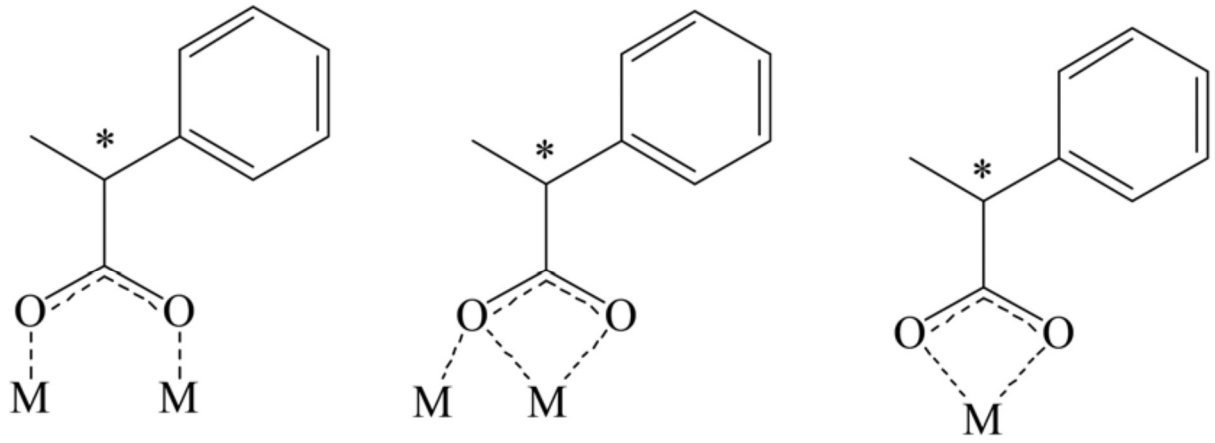

a) *syn, syn* bridge b) chelating-bridging c) chelating

FIGURE 3

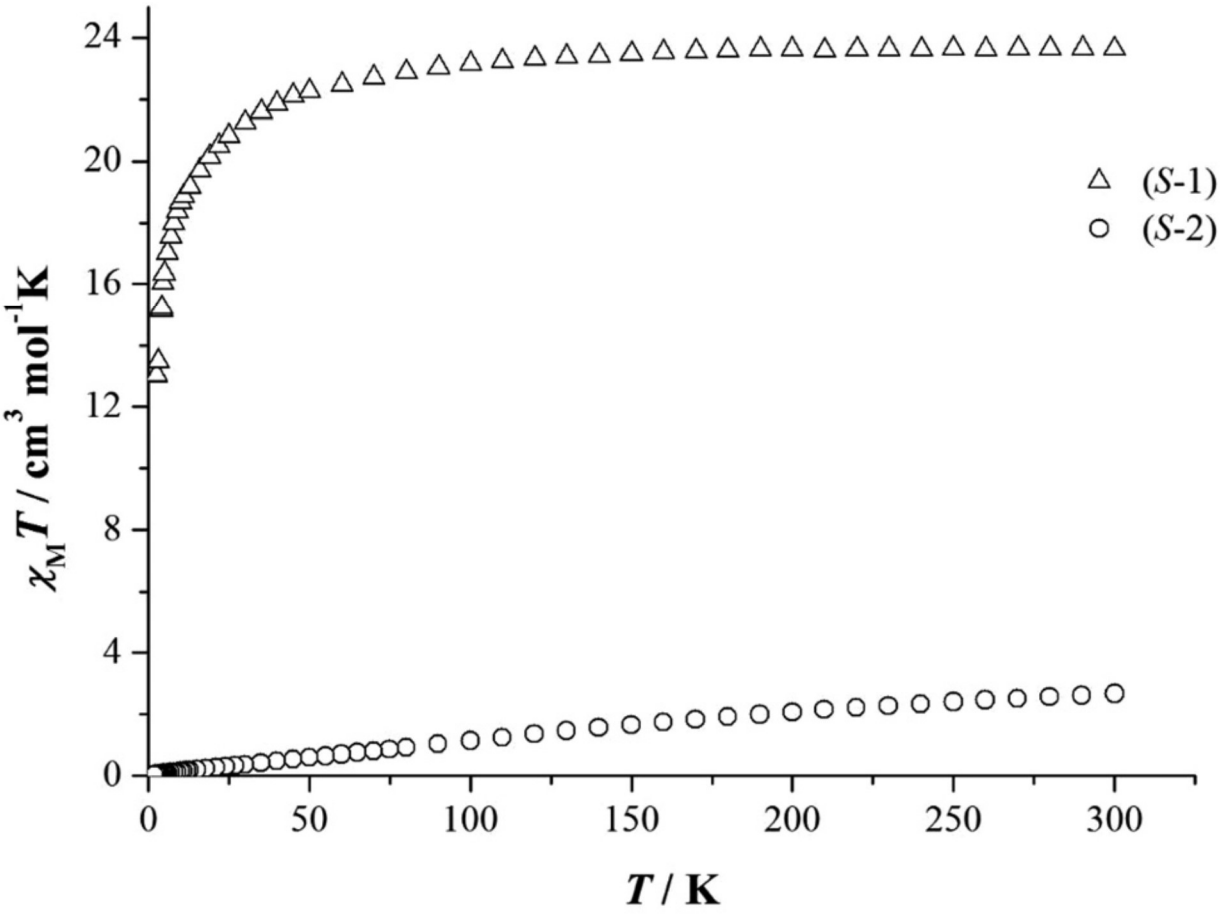

FIGURE 4

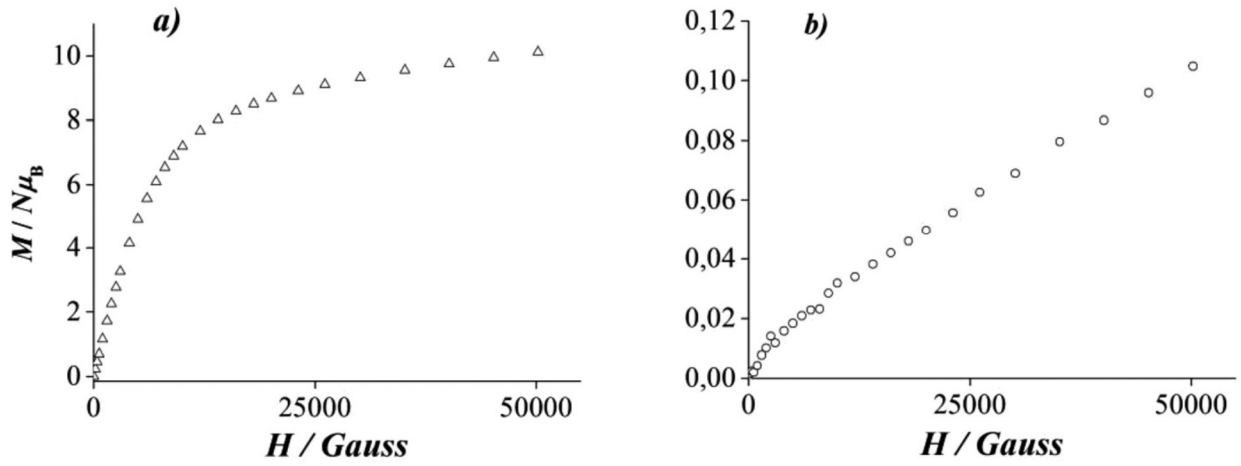
a)
M / Nμ_B
10
8
6
4
2
0
0
25000
50000
H / Gauss
b)
0,12
0,10
0,08
0,06
0,04
0,02
0,00
0
25000
50000
H / Gauss

FIGURE 5

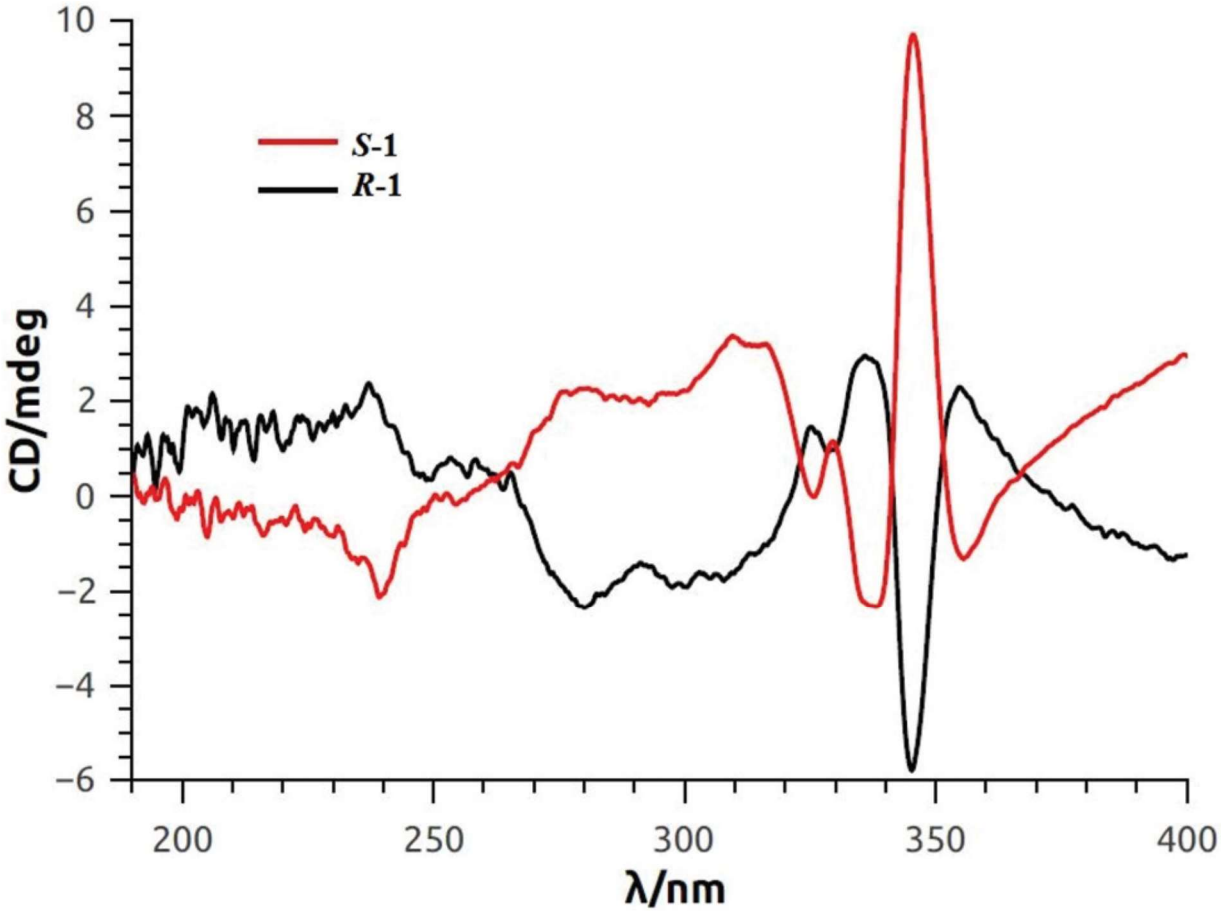

474 **FIGURE 6**

475

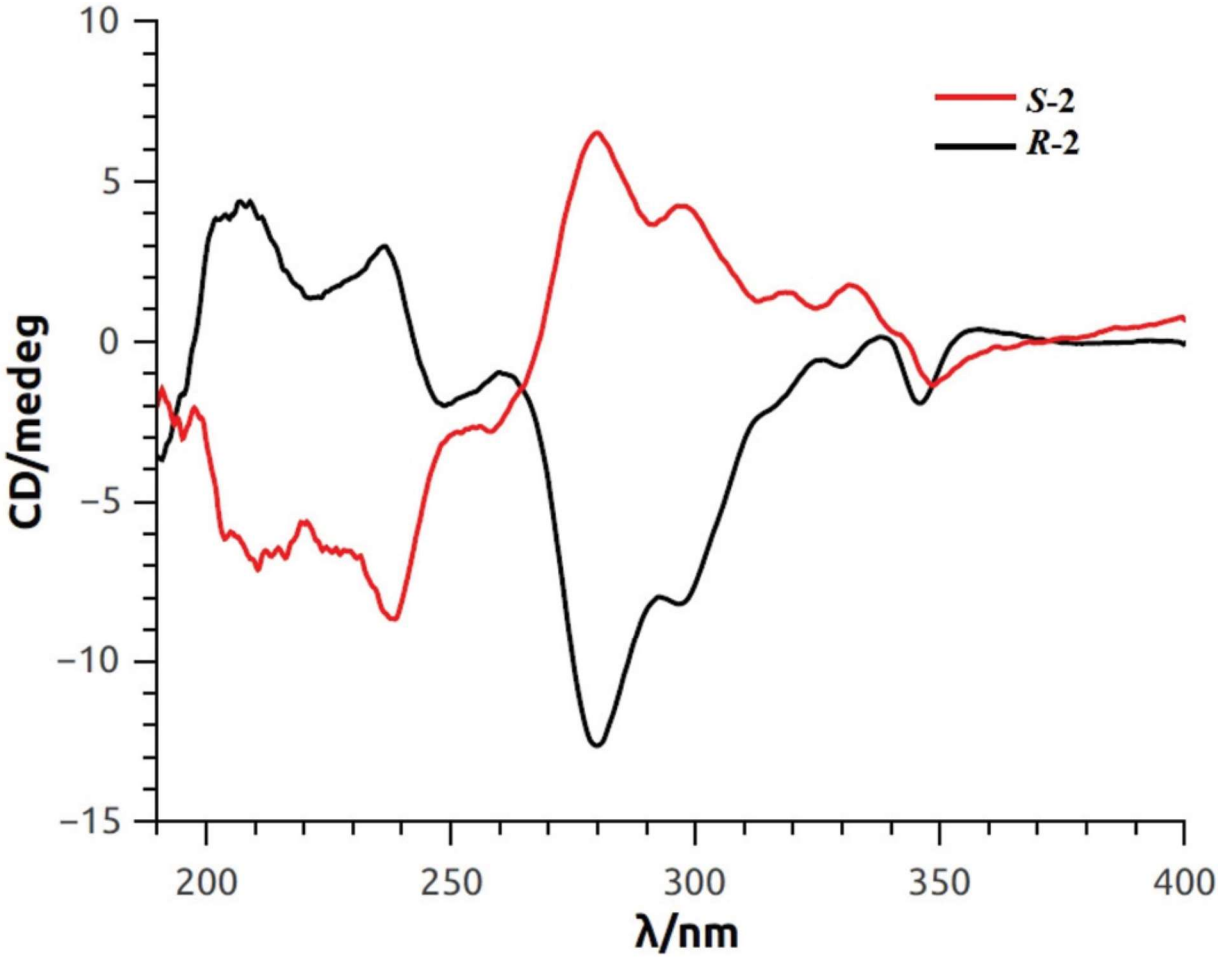

476

477

478 **FIGURE 7**

479
480

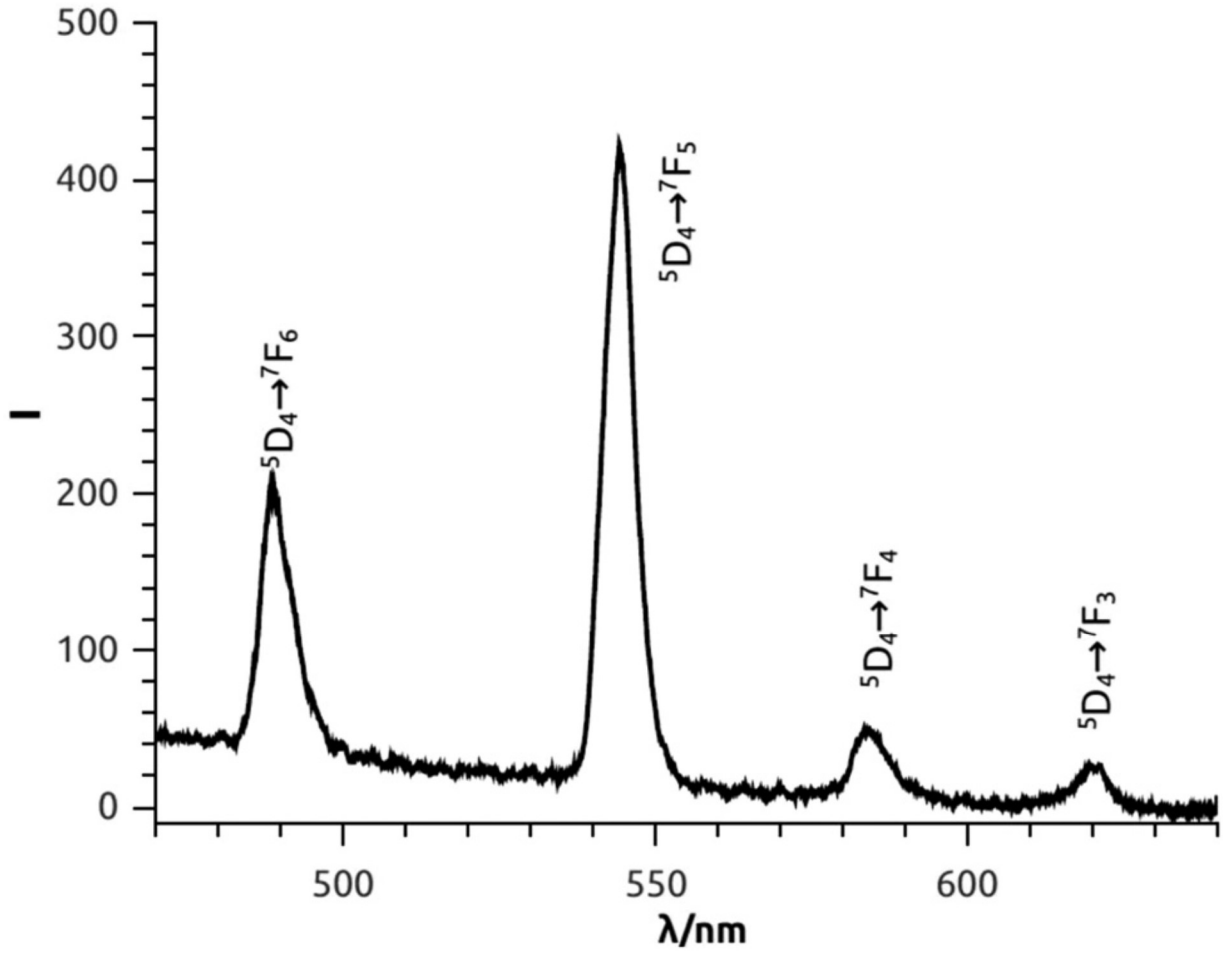

481
482
483

FIGURE 8

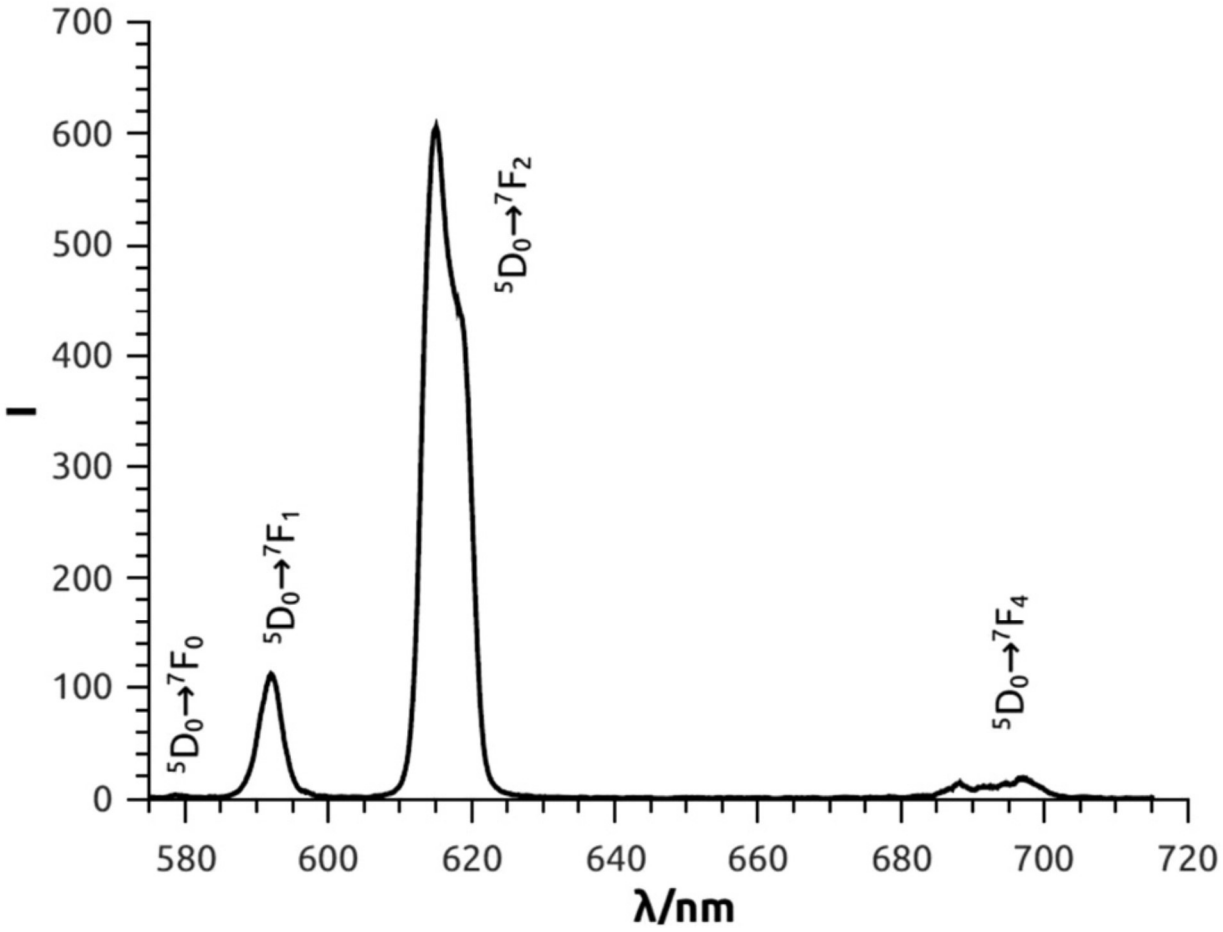
I
λ/nm
$^5D_0 \rightarrow {}^7F_0$
$^5D_0 \rightarrow {}^7F_1$
$^5D_0 \rightarrow {}^7F_2$
$^5D_0 \rightarrow {}^7F_4$
0
100
200
300
400
500
600
700
580
600
620
640
660
680
700
720

488 **FIGURE 9**

489
490

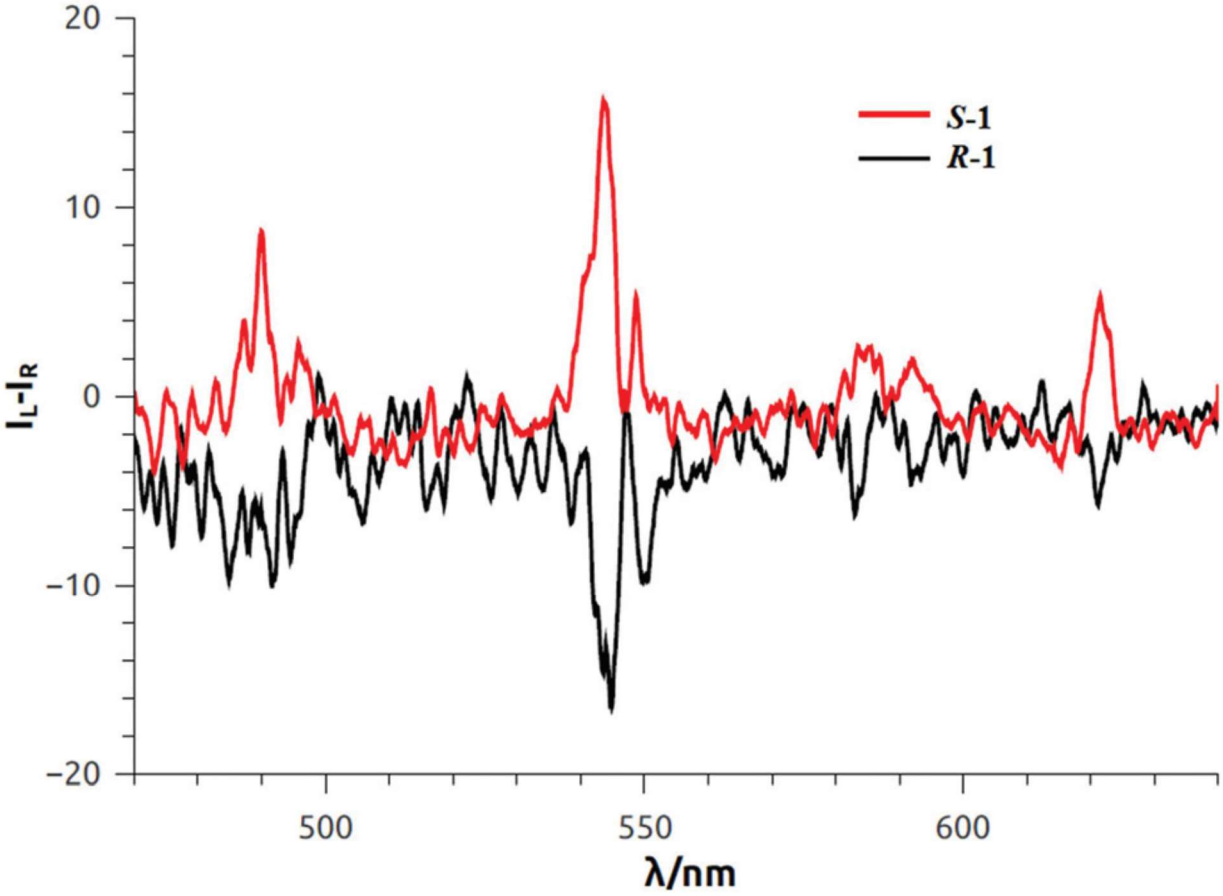

491
492
493

494 **FIGURE 10**

495

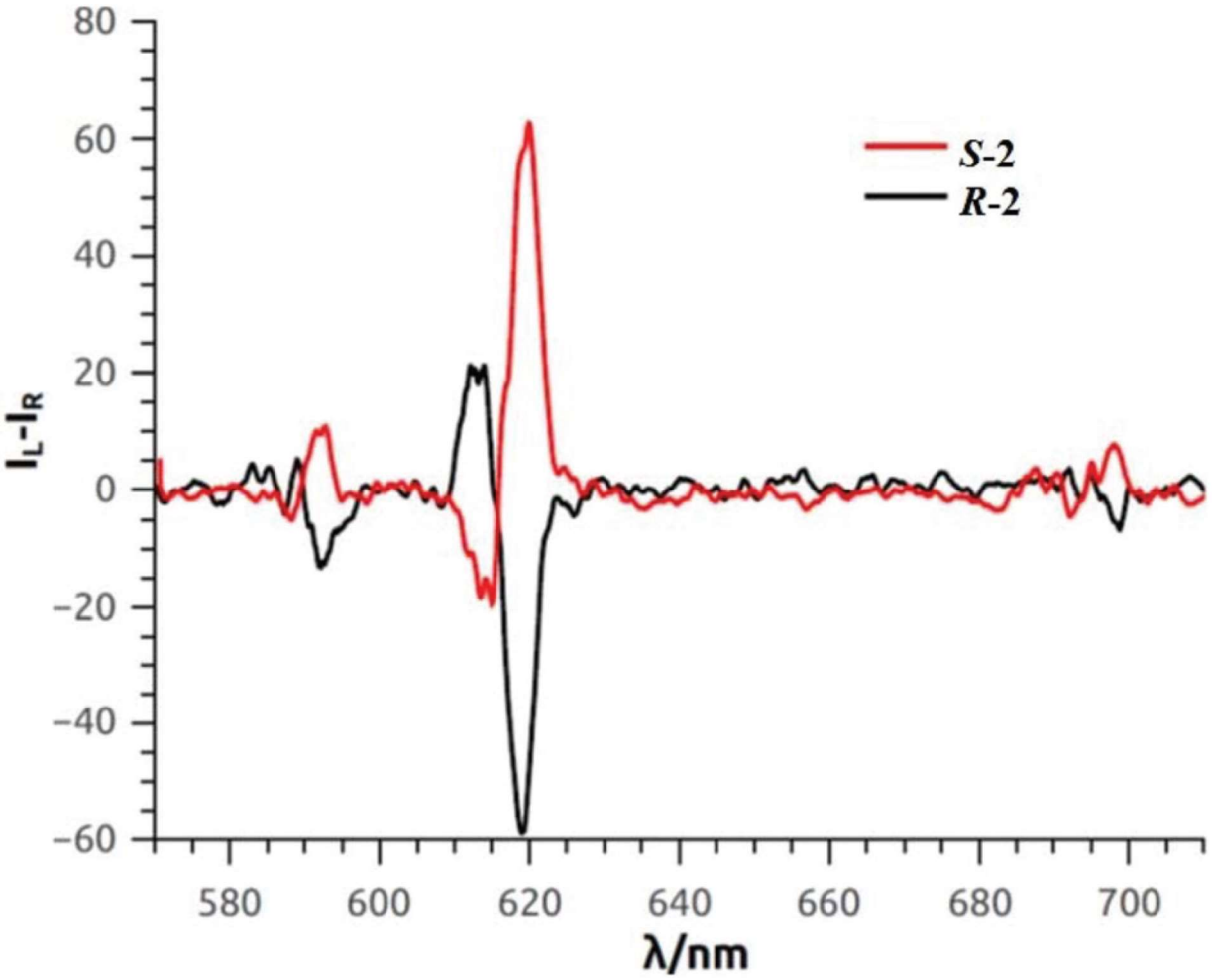

496
497

Table 1 Crystal data and collection details for the X-ray structure of complexes S/R-1–S/R-2

	S-1	*S*-2	*R*-1	*R*-2
Formula	$2\{C_{78}H_{70}N_4O_{12}Tb_2\}\cdot 5\{C_9H_{10}O_2\}$	$2\{C_{78}H_{70}N_4O_{12}Eu_2\}\cdot 5\{C_9H_{10}O_2\}$	$2\{C_{78}H_{70}N_4O_{12}Tb_2\}\cdot 5\{C_9H_{10}O_2\}$	$2\{C_{78}H_{70}N_4O_{12}Eu_2\}\cdot 5\{C_9H_{10}O_2\}$
FW	3897.34	3869.46	3897.34	3869.46
System	Monoclinic	Monoclinic	Monoclinic	Monoclinic
Space group	*P*21	*P*21	*P*21	*P*21
a/Å	17.6062(11)	17.5649(9)	17.5693(9)	17.5789(10)
b/Å	19.2507(12)	19.2624(10)	19.2449(10)	19.2932(11)
c/Å	26.6339(15)	26.7346(12)	26.6290(13)	26.7404(13)
α/°	90	90	90	90
β/°	99.980(2)	100.137(2)	99.938(2)	99.993(2)
γ/°	90	90	90	90
V/Å^3	8890.5(9)	8904.2(8)	8868.7(8)	8931.5(8)
Z	2	2	2	2
T, K	100(2)	100(2)	100(2)	100(2)
λ(MoKα), Å	0.71073	0.71073	0.71073	0.71073
D_{calcd}, (g cm^{-3})	1.4546	1.443	1.459	1.439
μ(MoKα), mm^{-1}	1.649	1.467	1.653	1.462
R	0.0427	0.0283	0.0394	0.0317
wR_2	0.0887	0.0493	0.0894	0.0695

503 **Table 2** Selected bond distances (Å) in the dinuclear fragment A for compounds S/R-1–S/R-2
504

	S-1	*S*-2	*R*-1	*R*-2
Ln1A–O1A	2.317(4)	2.341(3)	2.333(4)	2.361(3)
Ln1A–O3A	2.869(4)	2.806(3)	2.615(4)	2.606(3)
Ln1A–O4A	2.365(4)	2.394(3)	2.433(4)	2.466(3)
Ln1A–O5A	2.339(4)	2.364(3)	2.359(4)	2.388(3)
Ln1A–O7A	2.324(4)	2.349(3)	2.343(4)	2.382(3)
Ln1A–O9A	2.479(4)	2.488(3)	2.465(4)	2.479(3)
Ln1A–O10A	2.446(4)	2.469(3)	2.435(4)	2.462(3)
Ln1A–N1A	2.545(5)	2.587(4)	2.579(4)	2.604(3)
Ln1A–N2A	2.579(5)	2.576(4)	2.606(5)	2.630(3)
Ln2A–O2A	2.363(4)	2.395(3)	2.336(4)	2.369(3)
Ln2A–O3A	2.343(4)	2.370(3)	2.318(3)	2.352(2)
Ln2A–O6A	2.330(4)	2.342(3)	2.312(4)	2.343(3)
Ln2A–O7A	2.610(4)	2.596(3)	2.872(4)	2.821(3)
Ln2A–O8A	2.433(4)	2.465(3)	2.365(4)	2.401(3)
Ln2A–O11A	2.465(4)	2.477(3)	2.478(4)	2.500(3)
Ln2A–O12A	2.439(4)	2.463(3)	2.441(4)	2.476(3)
Ln2A–N3A	2.608(5)	2.623(4)	2.575(5)	2.598(3)
Ln2A–N4A	2.576(5)	2.588(4)	2.550(5)	2.576(3)
Ln1A···Ln2A	3.963	3.965	3.963	3.971

505
506

Table 3 glum factors for different transitions of the compounds S/R-1–S/R-2 on a quartz plate deposition

	$(R)\ g_{lum}$	$(S)\ g_{lum}$
Tb		
544 nm	-3.5×10^{-3}	$+3.5 \times 10^{-3}$
Eu		
593 nm	-9×10^{-3}	$+9 \times 10^{-3}$
613 nm	$+7 \times 10^{-3}$	-7×10^{-3}
620 nm	-1.2×10^{-2}	$+1.3 \times 10^{-2}$
698 nm	-1.8×10^{-2}	$+2.0 \times 10^{-2}$